High-pressure torsion of pure magnesium : Evolution of mechanical properties, microstructures and hydrogen storage capacity with equivalent strain

Edalati, Kaveh
Department of Materials Science and Engineering, Faculty of Engineering, Kyushu University | WPI International Institute for Carbon-Natural Energy Research, Kyushu University

Yamamoto, Akito
Department of Applied Chemistry, Faculty of Engineering, Kyushu University | WPI International Institute for Carbon-Natural Energy Research, Kyushu University

Horita, Zenji
Department of Materials Science and Engineering, Faculty of Engineering, Kyushu University | WPI International Institute for Carbon-Natural Energy Research, Kyushu University

Ishihara, Tatsumi
Department of Applied Chemistry, Faculty of Engineering, Kyushu University | WPI International Institute for Carbon-Natural Energy Research, Kyushu University

https://hdl.handle.net/2324/25496

High-pressure torsion of pure magnesium: Evolution of mechanical properties, microstructures and hydrogen storage capacity with equivalent strain

Kaveh Edalati,[a,c]* Akito Yamamoto,[b,c] Zenji Horita[a,c] and Tatsumi Ishihara[b,c]

[a] Department of Materials Science and Engineering, Faculty of Engineering, Kyushu University, Fukuoka 819-0395, Japan
[b] Department of Applied Chemistry, Faculty of Engineering, Kyushu University, Fukuoka 819-0395, Japan
[c] WPI International Institute for Carbon-Natural Energy Research, Kyushu University, Fukuoka 819-0395, Japan

Pure Mg (99.9%) is processed by high-pressure torsion (HPT) at room temperature. The hardness behavior with imposed strain is similar to pure Al (99.99%), having a hardness maximum followed by a steady state. HPT processing increases the hardness and tensile strength. A bimodal microstructure with an average grain size of ~1 μm is developed by HPT with some grains free of dislocations. Hydrogen absorption is improved by HPT after 10 revolutions, and a total hydrogen absorption of 6.9 wt.% is achieved.

*Corresponding author at: Department of Materials Science and Engineering, Faculty of Engineering, Kyushu University, Fukuoka 819-0395, Japan. Tel./fax: +81 92 802 2992; e-mail: kaveh.edalati@zaiko6.zaiko.kyushu-u.ac.jp

High-pressure torsion (HPT) is a severe plastic deformation (SPD) technique where a thin disc or ring is placed between two massive anvils under a high pressure and intense shear strain is introduced by rotating the two anvils with respect to each other [1,2]. It has been shown that the hardness after HPT processing is represented by a unique function of equivalent strain for various metals such as Al [2–7], Cu [8], Fe [9], Ti [10], Hf [11], V [12], and Mo [12]. However, the hardness behavior of pure Al is different from that of other pure metals. In most metals, a steady-state level is reached directly following an initial increase with straining [8–12]. However, in pure Al with a purity level of 99.99%, the hardness initially increases with increasing strain and, after reaching a maximum, decreases to a constant level [2–7]. Hardness–strain behavior similar to that of Al may be observed in pure Mg because both Al and Mg are similar in terms of melting temperature (T_m) and stacking fault energy (SFE) ($T_m = 933$ K for Al and 922 K for Mg, and SFE = 166 mJ.m^{-2} for Al and 125 mJ.m^{-2} for Mg [13]), and these parameters are the most important in terms of the deformation behavior. Thus, the first part of this study is to investigate the hardness behavior of pure Mg with respect to strain imposed by HPT.

In addition, the second part of this study examines hydrogen absorption behavior with HPT straining. It is well known that Mg produces a hydride in an atmosphere of hydrogen and Mg is considered a good candidate for a hydrogen storage material [14]. The main drawbacks of Mg in this respect are that its absorption and desorption temperatures are very high and the hydrogenation reaction is too slow. It is therefore important to look at how the absorption speed can be increased at low temperatures. The influence of SPD on the hydrogen storage performance of Mg alloys has been investigated in several papers and improvements in this respect have been reported after processing by equal-channel angular pressing (ECAP) [15–18] and HPT [19–23]. Moreover, it was shown that HPT is effective in formation of strain-induced hydride in pure Hf as well as in decreasing the dehydrogenation temperature [11]. However, little is understood to date regarding the hydrogen absorption behavior in high-purity Mg after processing by SPD. Since the alloying elements and their interaction with plastic strain may affect both thermodynamic and kinetic of hydrogen absorption, investigation of HPT-processed pure Mg is important to understand the effect of SPD, grain refinement and dislocation density on hydrogen storage capacity.

In this study, pure Mg is severely deformed by HPT and the evolution of mechanical properties and microstructures together with hydrogen storage performance are examined as a function of imposed strain.

Cylindrical rods of pure Mg (99.9%), 10 mm in diameter and 60 mm long, were cut from a 60x 80x180 mm^3 ingot. The rods were sliced to discs 0.8 mm thick using a wire-cutting electric discharge machine and further annealed for 1 h at 773 K under an argon atmosphere. HPT was conducted at room temperature using the annealed discs under a pressure of $P = 6$ GPa and subsequently shear strain was imposed through either $N = 0.25, 0.5, 1, 3$, or 10 revolutions with a rotation speed of $\omega = 0.5$ rpm. The HPT-processed discs were evaluated using Vickers microhardness measurement, tensile test, optical microscopy (OM), transmission electron microscopy (TEM) and hydrogen storage analysis.

First, after processing by HPT, the 10 mm discs were polished to a mirror-like surface and the Vickers microhardness was measured with an applied load of 50 g for 15 s along the radii from the center to edge at eight different radial directions at 0.5 mm increments.

Second, miniature tensile specimens with a gauge length of 1.5 mm, a width of 0.7 mm and a thickness of 0.5 mm were cut from the discs at a position 2 mm away from the center. Each tensile specimen was mounted horizontally on grips and pulled to failure using a tensile testing

machine with an initial strain rate of 2×10^{-3} s^{-1}. It should be noted that the dimensions of the present tensile specimens are fairly small, and therefore care is required when compared with other sizes of tensile specimens.

Third, for OM observations, the annealed discs were polished to mirror-like surfaces and etched in a solution of 5% HNO$_3$ and 95% C$_2$H$_5$OH.

Fourth, for TEM, 3 mm diameter discs were punched from the HPT discs at 3.5 mm away from the center. The 3 mm diameter discs were ground mechanically to a thickness of 0.15 mm and further thinned with a twin-jet electrochemical polisher using a solution of 2% HClO$_4$, 28% C$_3$H$_5$(OH)$_3$, and 70% CH$_3$OH at 263 K under an applied voltage of 30 V. TEM was performed at 200 kV for microstructural observation and for recording selected area electron diffraction (SAED) patterns.

Fifth, for hydrogen storage analysis, two discs were polished on both sides to a thickness of 0.55 mm and the hydrogen absorption rate was measured using a Sieverts type commercial gas adsorption apparatus (Bel Japan Inc., Bel Sorp HG) at 423 K. An approximate weight of 130 mg of the samples was exposed under a hydrogen pressure of 3MPa for 100 ks and the content of hydrogen absorbed in the sample was recorded every ~5 ks.

Figure 1a shows the variation in hardness with the distance from the centers of disc samples after 0.25–10 revolutions. The hardness variation is irregular and strongly depends on the extent of revolution. The hardness increases with respect to the distance from the center for 0.25 revolutions. The hardness increases, reaches a maximum and decreases as the distance from the center increases for 0.5 revolutions. However, the hardness exhibits a decrease with an increase in the distance from the center for 1, 3, and 10 revolutions.

To demonstrate the hardness behavior with respect to equivalent strain, all hardness values in Figure 1a are plotted against the equivalent strain in Figure 2b as attempted in earlier papers [2–12]. Here, the values of slippage fraction and thickness reduction during HPT were measured as described earlier [9,24]. Since both slippage and thickness reductions during HPT were negligible irrespective of the number of revolutions, the equivalent strain was calculated as:

$$\varepsilon = \frac{2\pi \, rN}{\sqrt{3} \, t} \tag{1}$$

where r is the distance from the disc center, N is the number of revolutions and t is the thickness of the disc. It is apparent that all data points now lie on a unique curve, reaching a maximum at an equivalent strain of 4, thereafter leveling off at an equivalent strain of ~20. This is then followed by the onset of a steady state where the hardness remained unchanged with straining. It should be noted that the hardness was plotted against the equivalent strain only up to $\varepsilon = 50$ in order to illustrate the variation in hardness at lower equivalent strain.

Despite the hexagonal close-packed (hcp) crystal structure of Mg, its hardness behavior after processing by HPT is very similar to that obtained in high-purity Al (99.99%), which as a face-centered cubic (fcc) crystal structure [2–7]. The mechanism for the unusual softening of pure Al at large strains was considered to be attributed to dynamic or fast static recovery due to easy cross-slip and/or dislocation climb arising from large SFE and low melting temperature [3,5]. In contrast to cubic metals, it is difficult for the cross-slip to occur in hcp metals because of crystallographic anisotropy and the limited number of slip systems. However, dislocation climb should be still active to promote the softening in Mg because diffusivity in Mg is high and the homologous temperature of 0.32 should be high enough to drive the recovery process.

The stress–strain curves are delineated in Figure 2 for HPT samples after 0.5 and 10

revolutions including an annealed sample. The sample after 0.5 revolutions corresponds to $\varepsilon = 5$ where the hardness reaches a maximum, and the sample after 10 revolutions corresponds to $\varepsilon = 90$ where the hardness remains in a steady state. In agreement with the hardness measurement shown in Figure 1, the ultimate tensile strength (UTS) is higher in the HPT sample after 0.5 revolutions than the annealed sample, but UTS slightly decreases as the number of revolutions increases to 10. The uniform elongation decreases with an increase in the number of revolution, but the total elongations to failure for the HPT samples are essentially comparable to that of the annealed sample. The high UTS and ductility obtained for the HPT samples indicate that the formation of cracks during deformation by HPT at room temperature is suppressed under high pressure.

An OM micrograph after annealing but before HPT is shown in Figure 3a and TEM micrographs including SAED patterns are shown in Figure 3b–h after HPT, where Figure 3b–e and g are TEM bright-field images, and Figure 3f and g are TEM dark-field images of Figure 3e and g, respectively, taken with the diffracted beams indicated by the arrows in the SAED patterns. The micrographs and corresponding SAED patterns were taken from three samples subjected to different magnitudes of the equivalent strain: Figure 3a shows annealed condition corresponding to $\varepsilon = 0$; Figure 3b $N = 0.25$ corresponding to $\varepsilon = 4$ where the hardness reaches a maximum; Figure 3c $N = 0.5$ corresponding to $\varepsilon = 8$ where the hardness decreases after reaching a maximum; Figure 3d $N = 1$ corresponding to $\varepsilon = 16$ where the hardness decreases before the onset of steady state; Figure 3e and f $N = 3$ corresponding to $\varepsilon = 50$ where the hardness reaches a steady state; and Figure 3g and h $N = 10$ corresponding to $\varepsilon = 160$ where the hardness is at a steady state.

Observation shows that the microstructure corresponding to Figure 3a consists of large grains with an average grain size of ~1600 μm after annealing. A texture develops and subgrains form in the shear direction in Figure 3b and many dislocations are visible within the grains where the hardness takes the maximum. Many dislocations are still visible within the grains in Figure 3c, but elongated grains are rarely seen within the microstructure and grain boundaries are ill-defined. The dislocation density is significantly reduced in Figure 3d and all grains are equiaxed. A bimodal microstructure is seen in Figure 3e and f and in Figure 3g and h, corresponding to the steady state. The bimodal microstructure at the steady state contains grains of submicrometer and micrometer size. Since few dislocations are visible within the micrometer-sized grains, they must be recrystallized. This is consistent with the idea that the hardness decrease at large strains is due to recrystallization because of the relatively low melting temperature of Mg. Statistical analysis at the steady state shows that 12% of grains have sizes less than 0.5 μm, 47% of grains are between 0.5 and 1 μm, 32% of grains are between 1 and 1.5 μm and 9% of grains are larger than 1.5 μm; the average grain size is ~1 μm. These microstructural features agree with the report by Bonarski et al. [25]. Although the smallest average grain size is achieved at the steady state, the highest hardness is obtained at $\varepsilon = 4$ because of the high dislocation density.

The HPT samples after $N = 0.25$ and 10 revolutions, including the annealed sample, were exposed to the hydrogen atmosphere under 3 MPa at 423 K. The amount of hydrogen absorption is then plotted in Figure 4 against the exposure time for the annealed and two HPT-processed samples. The sample after $N = 0.25$ corresponds to $\varepsilon = 4$ where the hardness reaches a maximum, and the sample after $N = 10$ corresponds to $\varepsilon = 160$ where the hardness has a steady-state value. Hydrogen absorption is small and there is almost no significant difference between the annealed sample and the HPT sample after $N = 0.25$ despite a large increase in the hardness. After $N = 10$, the hydrogen absorption becomes prominent and the absorption rate is significantly increased: it

is 12 times faster than those of the annealed sample and the sample after $N = 0.25$. The absorbed hydrogen was increased to 6.9 wt.% and this is fairly close to the maximum capacity of hydrogen storage in pure Mg (7.6 wt.%) [14]. It is considered that the improvement in the hydrogen absorption rate by HPT processing can be attributed to significant grain refinement and an increase in the area fraction of high-angle grain boundaries, because, as shown in Figure 3, the dislocation density appears to decrease with the number of revolutions. It is concluded that the HPT processing enhances the hydrogen storage capacity, and that high-angle grain boundaries play a more effective role than dislocations in the hydrogen absorption.

In summary, pure Mg (99.9%) was satisfactorily processed by HPT at room temperature and the following conclusions were obtained.
1. The hardness initially increases with increasing strain, reaches a maximum, and decreases to a steady-state level at large strains.
2. The softening at large strains is attributed to recrystallization because of relatively low melting temperature of Mg.
3. A bimodal microstructure including large recrystallized grains is observed at the steady state with an average grain size of _1 lm.
4. Following the HPT, the hardness, tensile strength, total elongation to failure and the hydrogen absorption improves.
5. The grain refinement is more important than dislocation density for the improvement of the hydrogen storage capacity.

[1] P.W. Bridgman, Phys. Rev. 48 (1935) 825–847.
[2] Y. Harai, Y. Ito, Z. Horita, Scripta Mater. 58 (2008) 469–472.
[3] C. Xu, Z. Horita, T.G. Langdon, Acta Mater. 55 (2007) 203–212.
[4] Y. Ito, Z. Horita, Mater. Sci. Eng. A 503 (2009) 32–36.
[5] K. Edalati, Y. Ito, K. Suehiro, Z. Horita, Int. J. Mater. Res. 100 (2009) 1668–1673.
[6] M. Kawasaki, B. Ahn, T.G. Langdon, J. Mater. Sci. 45 (2010) 4583–4593.
[7] M. Kawasaki, R.B. Figueiredo, T.G. Langdon, Acta Mater. 59 (2011) 308–316.
[8] K. Edalati, T. Fujioka, Z. Horita, Mater. Sci. Eng. A 497 (2008) 168–173.
[9] K. Edalati, T. Fujioka, Z. Horita, Mater. Trans. 50 (2009) 44–50.
[10] K. Edalati, E. Matsubara, Z. Horita, Metall. Mater. Trans. A 40 (2009) 2079–2086.
[11] K. Edalati, Z. Horita, Y. Mine, Mater. Sci. Eng. A 527 (2010) 2136–2141.
[12] S.W. Lee, K. Edalati, Z. Horita, Mater. Trans. 51 (2010) 1072–1079.
[13] J.P. Hirth, J. Lothe, Theory of Dislocations, second ed., McGraw-Hill, New York, 1968.
[14] B. Sakintuna, F. Lamari-Darkrim, M. Hirscher, Int. J. Hydrogen Energy 32 (2007) 1121–1140.
[15] V.M. Skripnyuk, E. Rabkin, Y. Estrin, R. Lapovok, Acta Mater. 52 (2004) 405–414.
[16] V.M. Skripnyuk, E. Rabkin, Y. Estrin, R. Lapovok, Int. J. Hydrogen Energy 34 (2009)

6320–6324.

[17] V. Skripnyuk, E. Buchman, E. Rabkin, Y. Estrin, M. Popov, S. Jorgensen, J. Alloys Compd. 436 (2007) 99–106.

[18] M. Zehetbauer, R. Grossinger, H. Krenn, M. Krystian, R. Pippan, P. Rogl, T. Waitz, R. Wurschum, Adv. Eng. Mater. 12 (2010) 692–700.

[19] Y. Kusadome, K. Ikeda, Y. Nakamori, S. Orimob, Z. Horita, Scripta Mater. 57 (2007) 751–753.

[20] G.F. Lima, A.M. Jorge Jr, D.R. Leiva, C.S. Kiminami, C. Bolfarini, W.J. Botta, J. Phys. Conf. Ser. 144 (2009) 012015.

[21] D.R. Leiva, D. Fruchart, M. Bacia, G. Girard, N. Skryabina, A.C.C. Villela, S. Miraglia, D.S. Santos, W.J. Botta, Int. J. Mater. Res. 100 (2009) 1739–1746.

[22] A. Revesz, Z. Kanya, T. Verebelyi, P.J. Szabo, A.P. Zhilyaev, T. Spassov, J. Alloys Compd. 504 (2010) 83–88.

[23] G.F. Lima, A.M. Jorge Jr, T.T. Ishikawa, J. Huot, D. Fruchart, S. Miraglia, C.S. Kiminami, W.J. Botta, Adv. Eng. Mater. 12 (2010) 786–792.

[24] K. Edalati, Z. Horita, T.G. Langdon, Scr. Mater. 60 (2009) 9–12.

[25] B.J. Bonarski, E. Schafler, B. Mingler, W. Skrotzki, B. Mikulowski, M.J. Zehetbauer, J. Mater. Sci. 43 (2008) 753–7518.

Figure Captions

Figure 1. Vickers microhardness plotted against (a) distance from center and (b) equivalent strain for disc samples processed after various numbers of revolutions.

Figure 2. Nominal tensile stress vs. nominal strain curves for annealed sample and samples processed by HPT for 0.5 and 10 revolutions.

Figure 3. OM micrograph for (a) annealed sample, and TEM micrographs and SAED patterns for disc samples processed by HPT for (b) 0.25, (c) 0.5, (d) 1, (e and f) 3, and (g and h) 10 revolutions; (f) is a dark-field image of (e), and (h) is a dark-field image of (g).

Figure 4. Amount of hydrogen absorption vs. exposure time in a hydrogen atmosphere for annealed sample and samples processed by HPT for 0.25 and 10 revolutions.
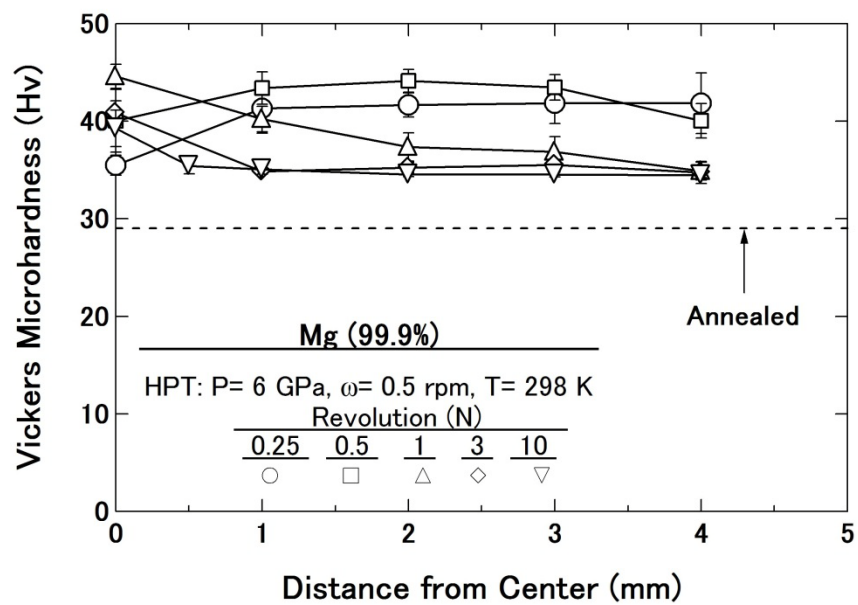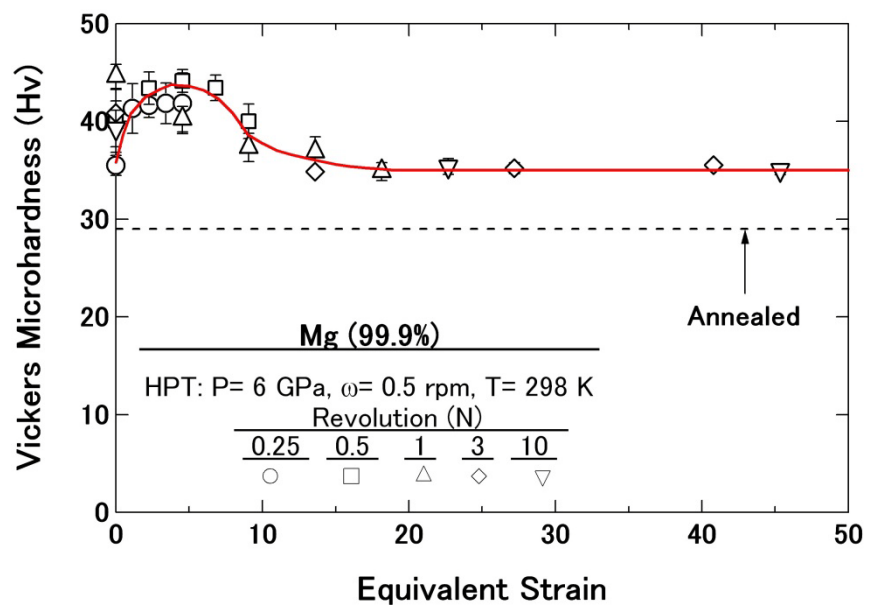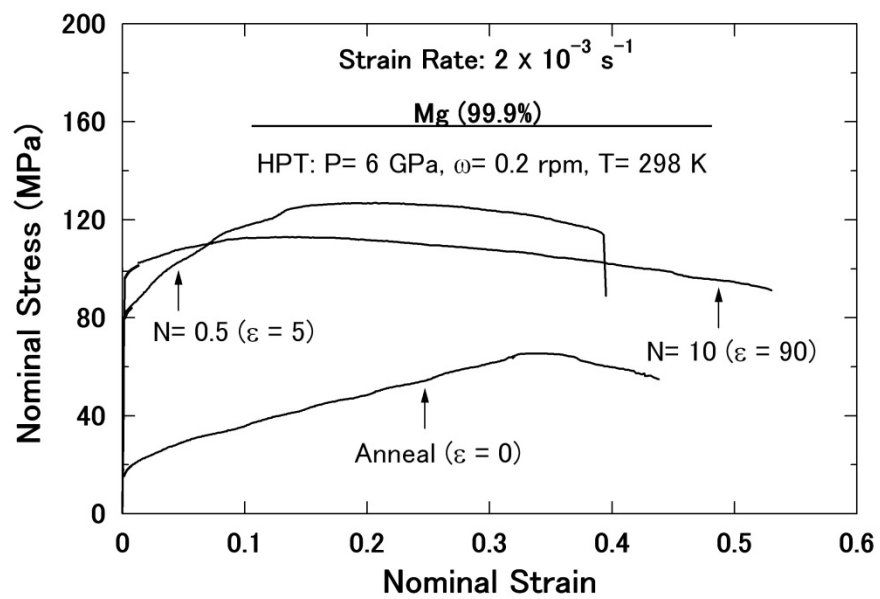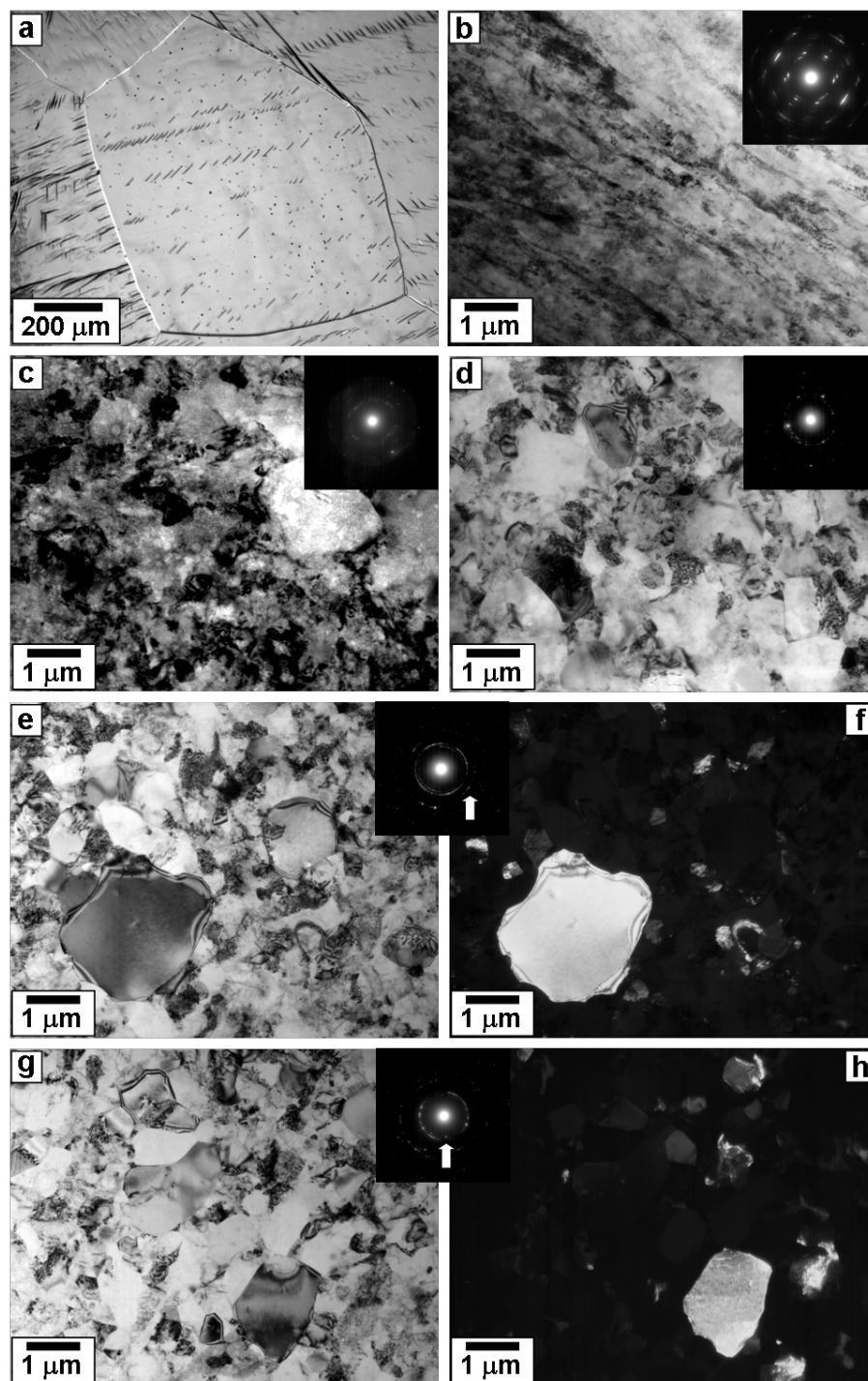
Figure 1a

Figure 1b

Figure 2

Figure 3

11

Figure 4